15TH IEA HEAT PUMP CONFERENCE
MAY 26–29, 2026 | HOFBURG
VIENNA 2026
DECARBONISATION THROUGH INNOVATION

Development of a test bench for characterizing the air-to-air heat pump of an electric vehicle

Marie Peeters[a,*], Elise Neven[a], Vincent Lemort[a], Samuel Gendebien[a]

[a]University of Liège, Thermodynamics Laboratory, Allée de la Découverte 17, 4000 Liège, Belgium

Abstract

This paper reports the experimental characterization of an air-to-air heat pump used in a B-segment electric vehicle, operating with R1234yf. The system consists of three heat exchangers (one outdoor and two integrated in the HVAC unit), a scroll compressor, valves, and an accumulator. This three-heat-exchanger architecture provides cabin cooling, heating, and dehumidification while avoiding refrigerant-flow reversal. The first part of the paper describes the design and commissioning of a dedicated experimental test bench conceived both as a didactic platform and as a research-oriented experimental facility for electric vehicle thermal management. Developed within a project-based learning framework, the bench was designed, assembled, and instrumented by Master's students in energy engineering. The heat pump components supplied by the vehicle manufacturer are presented, together with the operating modes, instrumentation layout, and measurement strategy. The second part presents experimental results obtained in cooling and heating modes over a wide range of compressor speeds and outdoor temperatures. The coefficient of performance is shown to strongly depend on temperature lift, decreasing from about 5 to 1.3 in cooling mode and from 3 to 1.8 in heating mode. Compressor isentropic and volumetric efficiencies are experimentally evaluated as functions of pressure ratio and pressure difference. The present study focuses on cabin thermal management; battery cooling is not implemented on the current bench configuration and is identified as a perspective for future work. A detailed uncertainty analysis confirms the robustness of the observed trends, despite higher uncertainties at low compressor speeds.

Keywords: Heat pump; Electric vehicle; HVAC; Experimental characterization; Thermal management; Test bench

1. Introduction

1.1. Context

According to the European Environment Agency (2025) [1], the transport sector is the largest source of greenhouse gas emissions in the European Union and has shown little progress in emission reduction in recent decades. In 2022, CO_2 emissions from road transport accounted for roughly 760 Mt CO_2, representing about 21% of the EU's total greenhouse gas emissions. One effort to change the trends is to increase the deployment of electric vehicle (EV) and promote the low-carbon fuels. According to [2] due to the comparatively short operational lifetime of vehicles relative to power plants, the land transport sector is capable of rapid transformation. In Denmark, for instance, electric vehicles represented approximately 51.5 % of newly registered passenger cars in 2024. In this context, there is growing interest in the thermal management of air conditioning (AC) systems, batteries, powertrain components, and other auxiliary equipment, as these systems significantly affect driving range, component lifetime, and overall efficiency, as highlighted by [3]. Air conditioning has become essential for ensuring driver comfort and safety. In EVs, however, it can substantially

* Corresponding author. Tel.: +32 495 81 03 94
E-mail address: marie.peeters@uliege.be

15th IEA Heat Pump Conference 2026 - TAP1.3 - https://doi.org/10.23697/0m73-3894

reduce battery range, representing a key limitation of the technology, as demonstrated by [4]. Optimizing these systems to minimize energy consumption is therefore critical. Unlike internal combustion engines, electric motors produce very little waste heat, leaving little energy available for cabin heating. To address this challenge, reversible heat pump systems have been developed, providing both cabin heating and cooling. These systems achieve considerably higher efficiency than conventional resistive heaters.

1.2. Motivation for research

Several experimental studies have investigated heat pump and air-conditioning systems for electric vehicles using dedicated test benches (Table 1). Most focus on specific objectives such as system performance evaluation, refrigerant substitution, operation under extreme ambient conditions, or integrated cabin–battery thermal management. These experimental platforms are primarily designed for research-oriented performance assessment or vehicle-level validation, and are generally optimized for a specific study objective.

Table 1. Experimental test benches for EV heat pump and air-conditioning systems

Refs	**Refrigerant**	**Operating modes**	**Battery thermal loop**	**Main scope**
[5]	R134a	Cooling	No	Experimental validation of AC system modeling
[6]	R134a	Cooling / Heating	No	Thermodynamic and exergetic evaluation of reversible AC/HP operation, performance limits and critical components
[7]	R134a	Cooling / Heating	No	Improvement of heating performance of EV heat pumps in cold climate conditions
[8]	R134a	Cooling / Heating/ Battery cooling / Battery preheating	Yes	Integrated thermal management of cabin and battery using heat pump and heat pipe technologies
[9]	R134a	Heating	No	Influence of control parameters on heating capacity, power consumption and COP, combined with exergy analysis
[10]	R134a	Cooling / Heating	No	Evaluation of automotive heat pump system performance and impact on EV driving range under extreme ambient temperatures
[11]	R1234yf	Cooling / Heating / Battery cooling	Yes	Experimental investigation of operating parameters and determination of optimal system settings for R1234yf-based EV HVAC systems
[12]	R1234yf / R134a	Cooling / Battery cooling	Yes	Experimental comparison of R1234yf and R134a and analysis of battery thermal load and compressor speed under realistic EV conditions
Present work	R1234yf	Cooling / Heating	No	Development of a modular, didactic test bench for a commercial EV air-to-air heat pump; comprehensive characterization of system and compressor performance over wide operating conditions; supports both education and research

This paper presents the development and characterization of a modular experimental test bench representing the reversible air-to-air heat pump system of a commercially available B-segment electric vehicle. The bench is designed for operation with R1234yf, without a battery thermal loop, and allows a complete performance assessment, including cooling and heating modes, overall system efficiency, and compressor behaviour across a wide range of operating conditions. The purpose of this study is to provide reference experimental data for reversible heat pump operation in EVs and to support both system understanding and future modelling or optimization efforts.

1.3. Motivation for educational purpose

In addition to research activities, the experimental bench was originally developed by first-year Master's students in Energy Engineering during the 2021–2022 academic year, with the primary objective of creating a practical and realistic teaching tool. It replicates the reversible air-to-air heat pump system of a B-segment electric vehicle and was developed in collaboration with a car manufacturer. The project illustrates the implementation of project-based and research-based learning approaches, as previously highlighted by [13] and [14].

While several experimental test benches for electric vehicle HVAC and heat pump systems have been reported in the literature, they are primarily designed for research-oriented performance evaluation or system optimization. In contrast, the present bench was specifically conceived as a modular and didactic platform, while remaining suitable for research use, enabling students to experimentally investigate heating and cooling operation, energy flows, and system efficiency under controlled laboratory conditions representative of real electric vehicle applications.

Currently, the bench serves as a hands-on laboratory tool at the Thermodynamics Laboratory of the University of Liège, supporting both educational activities and experimental research, and building on the benefits of experiential and active learning in engineering education, as highlighted by [15].

2. Materials and Methods

2.1. Test rig description

A solenoid valve system is employed to switch between operating modes, as directly reversing the refrigerant flow direction is physically impractical. This is due to several constraints: the calibrated orifice tube cannot handle refrigerant flow in both directions, and the internal heat exchangers in the HVAC system are dimensioned differently for each mode, preventing bidirectional operation.

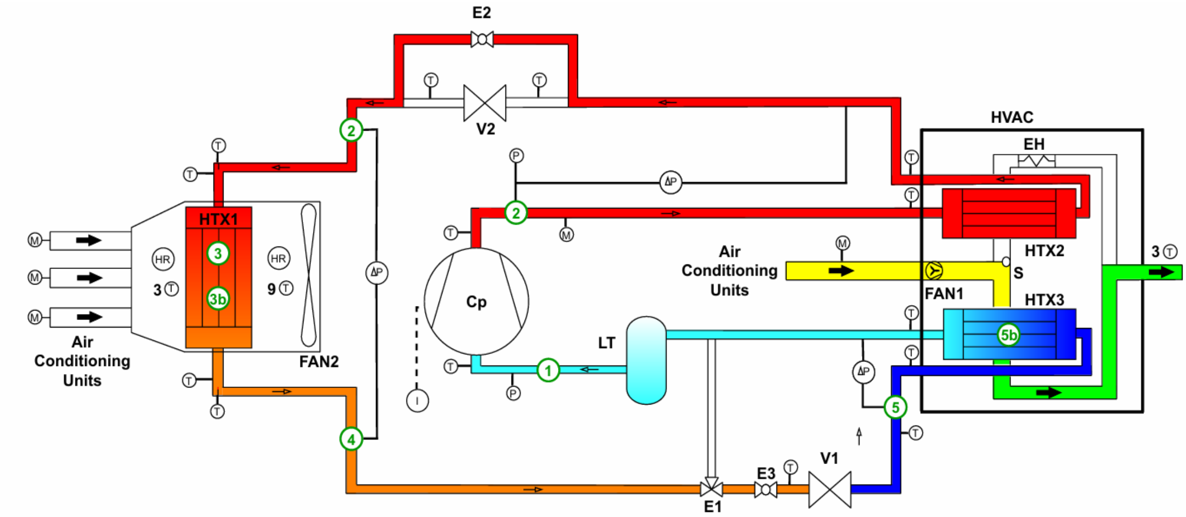

Figure 1. P&ID in cooling mode

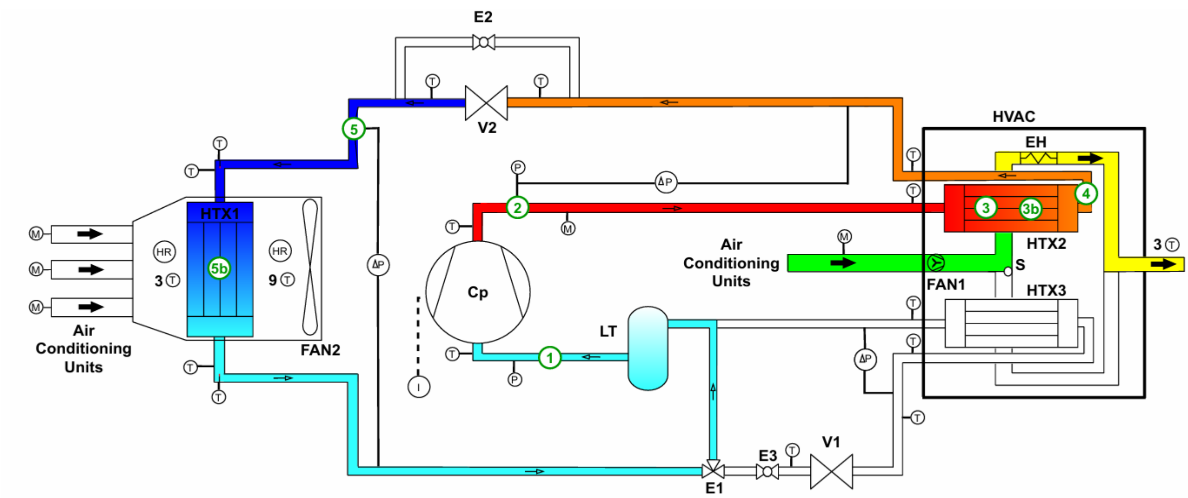

Figure 2. P&ID in heating mode

- **HTX1**: External heat exchanger
- **HTX2**: Inner condenser
- **HTX3**: Inner evaporator
- **HVAC**: Air conditioning unit of the car
- **Cp**: Compressor
- **LT**: Accumulator
- **E**: Electrovalves
- **V**: Orifice tubes
- **F**: Air fan
- **EH**: Electric heater
- **S**: Switch inside the HVAC

Measurements: (noted with a circle)

- Temperature (T)
- Absolute Pressure (P)
- Differential Pressure (ΔP)
- Current (I)
- Flow meter (M)
- Relative Humidity (HR)

Air flows directions are represented by ➡

All components of the test bench replicate those of a commercially available B-segment electric vehicle's reversible heat pump system. The only exception is the compressor, which is a PWM-controlled scroll unit with a larger displacement (34 cm^3 vs. 27 cm^3) [16].

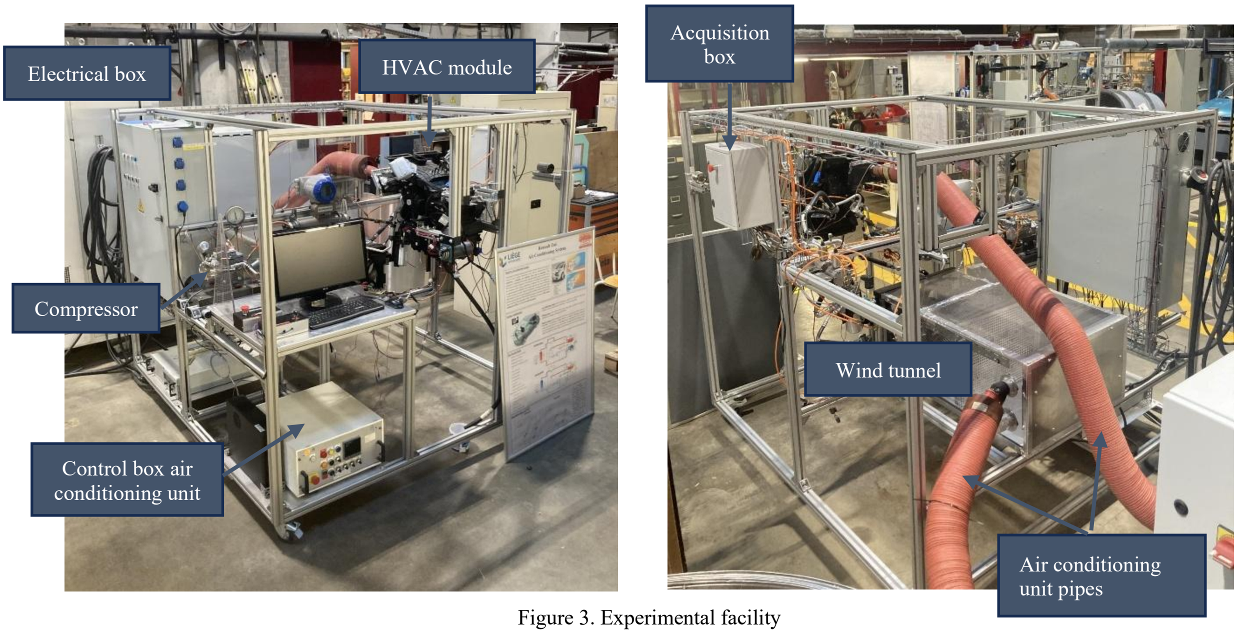

Figure 3. Experimental facility

To conduct experimental tests and emulate real driving conditions, a portable air conditioning unit has been selected. This unit can deliver variable airflow rates and temperatures within the ranges of 0-600 m^3/h and 0-60 °C, respectively. It has two air outlets: one directly connected to the HVAC module and the other to a wind tunnel. This wind tunnel is designed to replicate the airflow conditions encountered by a vehicle's front heat exchanger. The external heat exchanger (HTX1) and front fan (FAN2) are installed within the tunnel. Depending on the system configuration, HTX1 functions as a condenser in cooling mode and as an evaporator in heating mode.

2.2. Measurement techniques

Several sensors are also installed for the measurement of temperature, pressure, humidity, mass flow rate, and electrical consumption. Thermocouples are placed at different locations, including some on the surface and others in immersion sleeves. Absolute and differential pressure sensors are used to measure absolute pressures and pressure drops across the exchangers. A relative humidity sensor is added downstream of HTX1 for operation as an evaporator. Finally, a Coriolis flow meter and a current sensor are used for mass flow rate and electrical power measurement.

Table 2. Bench sensors characteristics

Parameter	Type	Range	Accuracy
Temperature	Type T thermocouples	[-270;370] °C	±1K
Pressure	Absolute	[0;30] bar	±0.02 bar
		[0;10] bar	±0.05 bar
	Differential	[0;1] bar	±2.5 mbar
		[0;0.5] bar	±5 mbar
Relative humidity	Humidity sensor	[0;100] %	±2% r.h
Working fluid mass flow	Coriolis	[0;1230] kg/h	±0.1% m.v.
DC current	Current sensor	[0;25] A	±0.7% f.s.

The uncertainties of the reported findings are evaluated from the known sensor accuracies using a method described in [17]. The purpose of this technique is to calculate how the uncertainty in each of the directly measured variables $x_1, x_2, \dots, x_n$ propagates into the value of the calculated quantity $y = f(x_1, x_2, \dots, x_n)$. According to this method, the uncertainty of the calculated quantity (U_y) can be determined as a function of the measured variables' uncertainties $(U_{x,i})$ via:

$$U_y = \sqrt{\sum_{i=1}^{n} \left(\frac{\partial y}{\partial x_i}\right)^2 \cdot {U_{x,i}}^2} \quad (1)$$

2.3. Experimental controlled parameters

Several parameters can be adjusted on the test bench in order to reproduce various operating scenarios and simulate different environmental or vehicle conditions. Four main parameters can be independently controlled:

- <u>Compressor speed</u>: As previously mentioned, the compressor rotational speed is controlled by modifying the duty cycle of a PWM signal. This duty cycle can be directly entered through the LabVIEW interface, which then sets the corresponding compressor speed. This allows precise adjustment of the refrigerant mass flow rate

- <u>Outdoor air temperature</u>: To simulate different ambient conditions encountered by the vehicle, the outlet air temperature of the portable air conditioning unit can be adjusted using its dedicated control box. The temperature can be set within a range of 0 to 60 °C, allowing the reproduction of both winter and summer operating conditions.

- <u>Airflow through the HVAC module</u>: The fan speed of the portable air conditioning unit can be adjusted using a potentiometer graduated from 1 to 10. It is also possible to distribute the airflow between the two outlets of the unit. Although the unit provides a maximum nominal airflow of 600 m^3/h, pressure losses along the ducts reduce the effective flow rate at the HVAC inlet. In addition, the speed of the internal blower (FAN1) within the HVAC module can be controlled by varying the duty cycle of its PWM signal, thus allowing fine adjustment of the airflow across the internal heat exchangers.

- <u>Airflow through the external heat exchanger (HTX1)</u>: The second outlet of the portable air conditioning unit supplies air to the wind tunnel, which directs the flow toward the front heat exchanger (HTX1) to reproduce ram effect due to driving conditions. The speed of the FAN2 can also be controlled by adjusting the duty cycle of its PWM signal, enabling regulation of the airflow rate across HTX1 and, consequently, the external heat transfer conditions.

2.4. Facility characterization & validation

Accurate knowledge of the airflow rates through the heat exchangers is essential for the proper characterization of the test bench. This section focuses on how the airflow was measured through the different exchangers, namely the front heat exchanger (HTX1) and the internal condenser (HTX2) and evaporator (HTX3), both located inside the HVAC module.

2.4.1. Anemometer

For the front heat exchanger (HTX1), air velocity was measured at nine locations. During this test, both the front fan (FAN2) and the internal fan of the portable unit were operating at their maximum speed. By averaging the measurements from the nine points, the airflow through HTX1 could be estimated.

For HTX2 and HTX3, located inside the HVAC module, air velocity was measured at three locations at the HVAC outlet. In this case, the blower (FAN1) and the internal fan of the portable unit were running at their maximum speed. By averaging the three measurements, the maximum airflow leaving the HVAC module could be estimated.

2.4.2. Orifice plate

As an alternative method to measure the airflow at the HVAC outlet, an orifice plate was installed. Under normal test conditions, i.e., with the airflow to the HVAC module set at maximum. This method only applies to the airflow leaving the HVAC, thus for HTX2 and HTX3.

2.4.3. Heat balance on the heat exchanger

The air mass flow rate can also be determined using a heat balance on the heat exchangers. For a condenser, no condensation occurs on the air side, and only sensible heat transfer is involved. In this case, the thermophysical properties of humid air can be used without accounting for latent heat effects. For an evaporator, however, condensation occurs and latent heat transfer must be taken into account. To address this, relative humidity sensors are placed upstream and downstream of HTX1. Unfortunately, it was not possible to install humidity sensors for HTX2 due to the difficult accessibility inside the HVAC module.

2.4.4. Comparison of airflow measurement methods

Table 3 summarizes the airflow rates obtained with the different measurement methods for HTX1 and for the HVAC module (HTX2 and HTX3). The portable air-conditioning unit used in the setup is nominally capable of delivering an airflow of approximately 600 m³/h. Since this airflow is distributed between two outlets, an airflow on the order of 300 m³/h could be expected for both the wind tunnel (HTX1) and the HVAC module, depending on the respective pressure losses. In practice, the measured values are significantly lower due to substantial pressure losses between the air-conditioning unit and the wind tunnel, as well as between the unit and the HVAC module.

In addition, most of the multiple inlet and outlet ports of the HVAC module were sealed in order to enforce a single inlet–outlet path. Despite this, air leakage still occurs through the remaining imperfectly sealed paths, and internal recirculation within the module further reduces the effective airflow.

Table 3. Airflow measurements

	$\dot{V}_{air,HTX1}$ $[m^3/h]$	$\dot{V}_{air,HVAC}$ $[m^3/h]$
Anemometer	260	60
Orifice plate	\	50
Heat balance (cooling mode)	450	250
Heat balance (heating mode)	220	160

For HTX1, the airflow rate measured with the anemometer is consistent with the value obtained from the heat balance in heating mode.

For the HVAC module, the anemometer and orifice-plate measurements show good agreement. In contrast, the airflow rate estimated from the heat balance is more difficult to interpret, since HTX2 and HTX3 are located within the core of the HVAC module and the temperature measurements are taken only at the module outlet, after some degree of air mixing and recirculation has already occurred. In addition, no humidity sensor was available for the evaporator (HTX3), preventing a reliable enthalpy-based heat balance. This configuration makes it inherently challenging to obtain a representative heat balance for these exchangers.

Overall, estimating the airflow rate through the heat exchangers in both operating modes is difficult due to these limitations, and only rough approximations could be obtained.

2.5. Experimental matrix

The objective of the experimental campaign was to perform a series of tests in both heating and cooling modes in order to analyse the influence of key controllable parameters such as outdoor air temperature and compressor rotational speed. Due to significant pressure losses along the air ducts, the airflow rates through the HVAC module and the external heat exchanger were kept constant at their maximum achievable values. Consequently, the fan of the portable air conditioning unit and both fans (FAN1 and FAN2) operated at full speed during all tests.

For safety reasons, the compressor speed is limited so that the outlet pressure does not exceed 25 bar. In this work, the properties of the refrigerant–oil mixture are not considered.

A total of fifteen tests were carried out in cooling mode, covering three different outdoor air temperatures (25, 35, and 45 °C) and five compressor speeds. For heating mode, due to the safety limit imposed on the compressor outlet pressure, only a limited number of tests could be performed. Nine tests were conducted for three outdoor temperatures (0, 5, and 10 °C) and three compressor speeds. The main operating conditions for all tests are summarized in Fig. 4.

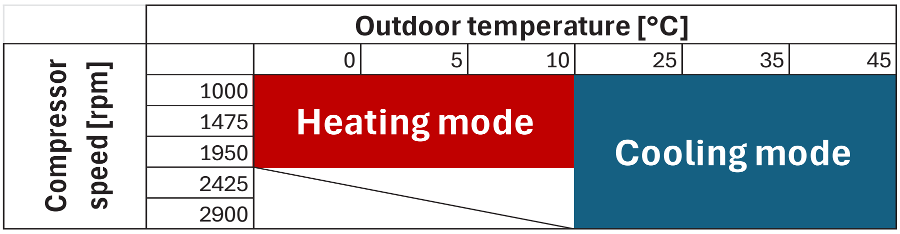

Figure 4. Experimental test matrix

2.6. Data reduction for KPI determination

This section introduces the performance indicators used to evaluate both the components and the overall cycle performance discussed in Section 3.

2.6.1. Cycle

For a reversible heat pump, the main performance metric is the coefficient of performance (COP). It is defined as the ratio of the useful heat transfer rate by the system to the electrical power consumed by the compressor. In cooling mode, the useful heat transfer is produced by the evaporator. The COP is expressed as follow:

$$COP_{cooling} = \frac{\dot{Q}_{ev}}{\dot{W}_{el,cp}} \tag{2}$$

On the other hand, in heating mode, it is the amount of heat released by the condenser which represents the useful energy:

$$COP_{heating} = \frac{\dot{Q}_{cd}}{\dot{W}_{el,cp}} \tag{3}$$

Another key parameter is the temperature lift, defined as the difference between the saturation temperatures corresponding to the condensation and evaporation pressures [18]. These pressures are measured at the compressor outlet and inlet, respectively. Pressure drops across the heat exchangers are monitored using differential pressure sensors and are therefore accounted for in the analysis.

$$\Delta T_{lift} = T_{sat}(p_{cd}) - T_{sat}(p_{ev}) \tag{4}$$

2.6.2. Component performance

The main criterion for evaluating volumetric machine performance is the isentropic efficiency, defined as follows:

$$\eta_{is} = \frac{\Delta h_{is}}{\Delta h_{real}} \tag{5}$$

However, this definition assumes no ambient losses, which is far from the case for real volumetric machine operating in this experimental setup. Therefore, a more practical definition is used:

$$\eta_{is} = \frac{\dot{m}_{ref}\,\Delta h_{is}}{\dot{W}_{el,cp}} \tag{6}$$

where $\dot{m}_{\mathrm{wf}}$ is the refrigerant mass flow rate and $\dot{W}_{\mathrm{el,cp}}$ is the electrical power consumption of the compressor. This formulation accounts for real-world losses, as well as the effect of oil circulation within the compressor, providing a more representative measure of performance on the experimental bench.

Another important performance metric for compressors is the volumetric efficiency, which relates the measured volume flow rate at the compressor inlet to the theoretically displaced volumetric flow rate (using swept volume). This metric provides an indication of internal leakages within the machine as well as suction pressure drop and heat transfer.

$$\eta_{\mathrm{vol}} = \frac{\dot{V}_{\mathrm{su}}}{\dot{V}_{\mathrm{su,id}}} = \frac{\dot{m}_{ref}}{n_{\mathrm{cp}}\,.V_{\mathrm{s,cp}}.\rho} \tag{7}$$

3. Results and Discussion

This section presents the results of several experimental campaigns conducted according to the test matrix shown in Fig. 4.

3.1. Cycle

Fig. 5 and Fig. 6 show the evolution of the COP as a function of the temperature lift for both cooling and heating modes respectively. The COP in cooling mode is calculated using Eq. (2), and the COP in heating mode using Eq. (3). The temperature lift, defined as the difference between the condensation and evaporation saturation temperatures, is computed using Eq. (4).

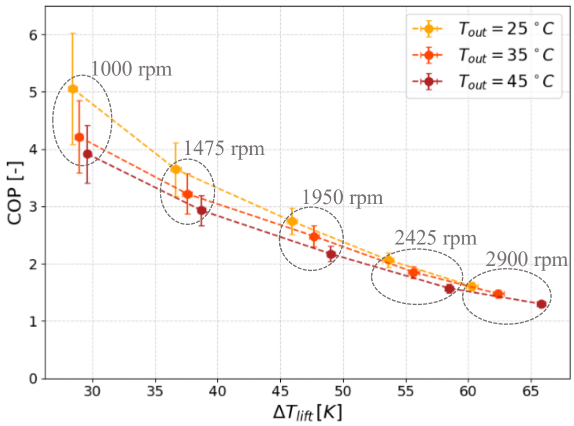

Figure 5. COP vs. ΔT_{lift} for different outside temperatures (cooling mode)

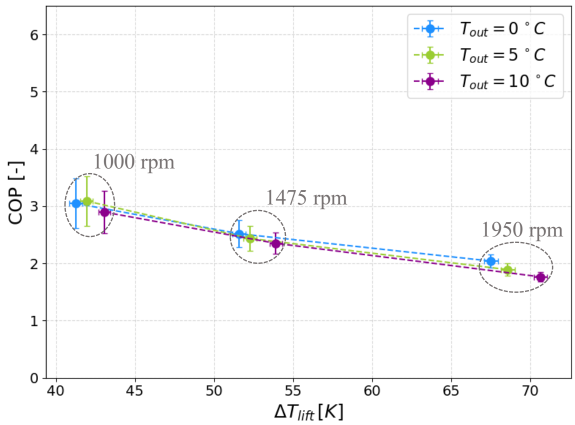

Figure 6. COP vs. ΔT_{lift} for different outside temperatures (heating mode)

For both operating modes, a decrease in COP is logically observed as the temperature lift increases. This trend is expected since a higher temperature lift requires the compressor to operate over a larger pressure ratio, resulting in a higher compression work for the same useful heat output.

In cooling mode, for a given compressor speed, a degradation of the COP is observed when the outdoor temperature increases. In this case, comparing COP values at identical temperature lifts is not always possible because higher outdoor temperatures naturally lead to higher condensation pressures and saturation temperatures, and thus to different temperature lifts. This behaviour is logical: the system operates more efficiently at low outdoor temperatures. Experimentally, the COP decreases from approximately **5** at a temperature lift of **28 K** (Tout = 25 °C) down to about **1.3** at a temperature lift of **65 K** (Tout = 45 °C).

In heating mode, a slightly higher COP is obtained at lower outdoor temperatures for identical compressor speeds. Again, this is explained by the fact that the temperature lifts are not the same for the different outdoor conditions, since lower ambient temperatures reduce the saturation temperature at the evaporator, increasing the system efficiency. The COP decreases from approximately **3** at a temperature lift of **41 K** (Tout = 0 °C) to around **1.8** at a temperature lift of **70 K** (Tout = 10 °C).

The uncertainties of COP and temperature lift were calculated using Eq. (1). The main contribution to COP uncertainty comes from the current measurement. At low compressor speeds, corresponding to low electrical power, this error has a larger relative impact, leading to COP uncertainty in cooling mode up to ~0.97 at 28 K and 1000 rpm. COP uncertainty decreases as compressor speed increases, while temperature lift uncertainty remains small, below 0.5 K across the tested range. These trends indicate that, despite higher uncertainty at low speed and lift, the overall decrease of COP with increasing temperature lift is robust.

Fig. 7 and Fig. 8 show the thermal and electrical powers as a function of temperature lift for cooling and heating modes, respectively, with maximum values of approximately **2.1 kW** for the evaporator at Tout = 45 °C (cooling mode) and **2 kW** for the condenser at Tout = 10 °C (heating mode).

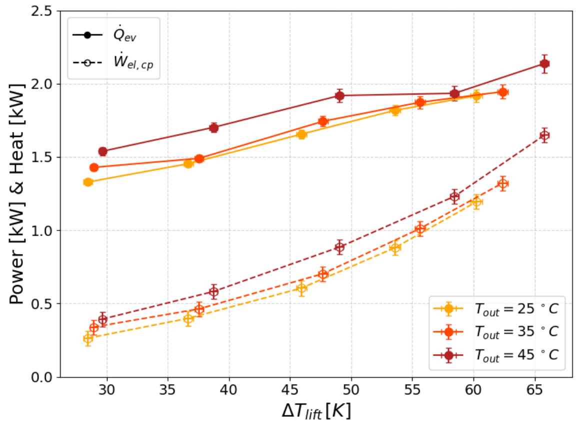

Figure 7. $\dot{Q}_{ev}$ & $\dot{W}_{el,cp}$ vs. ΔT_{lift} for different outside temperatures (cooling mode)

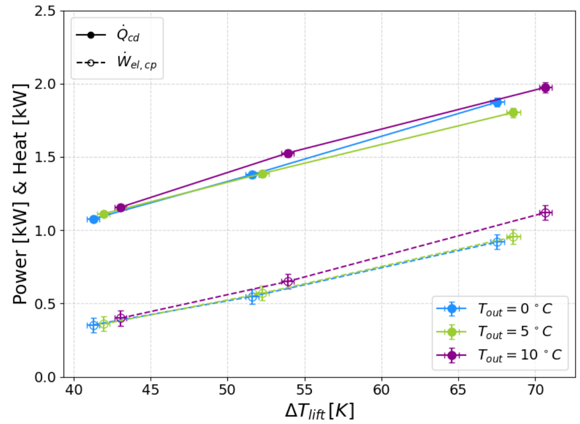

Figure 8. $\dot{Q}_{cd}$ & $\dot{W}_{el,cp}$ vs. ΔT_{lift} for different outside temperatures (heating mode)

3.2. Compressor performance

The performance of the scroll compressors was evaluated in terms of isentropic and volumetric efficiencies as functions of the pressure ratio and pressure difference, respectively. Fig. 9 (cooling mode) and Fig. 10 (heating mode) show the isentropic efficiency calculated with Eq. (6), plotted as a function of the pressure ratio.

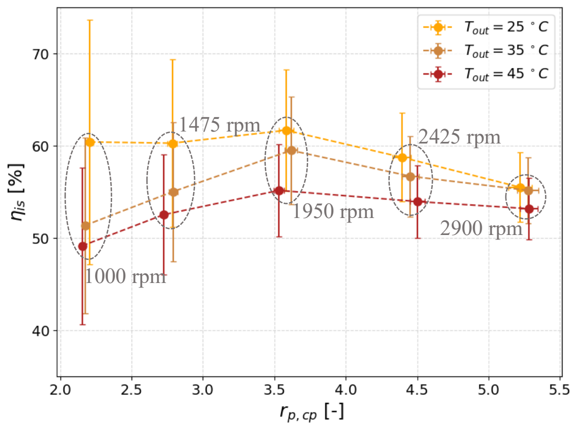

Figure. 9. Isentropic efficiency calculated with Eq. (6) vs. pressure ratio for different outside temperatures (cooling mode)

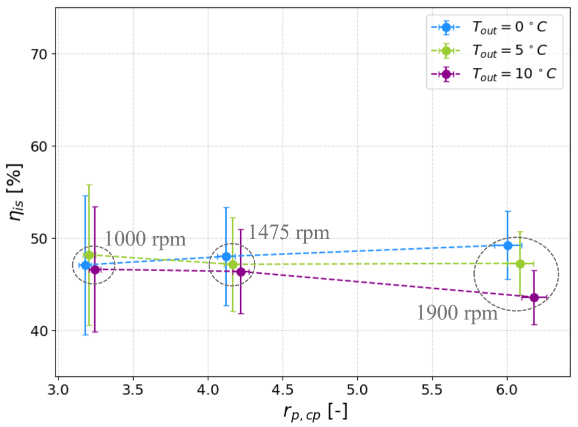

Figure. 10. Isentropic efficiency calculated with Eq.(6) vs. pressure ratio for different outside temperatures (heating mode)

In cooling mode, a maximum isentropic efficiency of approximately **60%** is observed for an outdoor temperature of 25 °C at the lowest compressor speed. In heating mode, the maximum efficiency reaches about **49%** for an outdoor temperature of 0 °C at a compressor speed of 1900 rpm. When calculating isentropic efficiency using Eq. (6), the result depends on the compressor electrical power and is therefore affected by the current measurement uncertainty. Consequently, higher uncertainties are observed at low compressor speeds and low pressure ratios, reaching up to about 13% in cooling mode at 1000 rpm and an outdoor temperature of 25 °C, and decreasing as compressor speed and pressure ratio increase.

The volumetric efficiency of the scroll compressor is shown as a function of the pressure difference for different compressor speeds in cooling mode (Fig. 11) and heating mode (Fig. 12). The observed trends can be explained by the competing effects of compressor speed and pressure difference. Increasing the rotational speed tends to reduce the effect of internal leakage, thereby improving volumetric efficiency. Conversely, a higher pressure difference increases leakage through the clearances, which reduces volumetric efficiency. At low speeds, the effect of the increasing pressure difference dominates, leading to a slight decrease in volumetric efficiency. At higher speeds, the beneficial effect of increased rotational speed becomes dominant, resulting in an increase in volumetric efficiency.

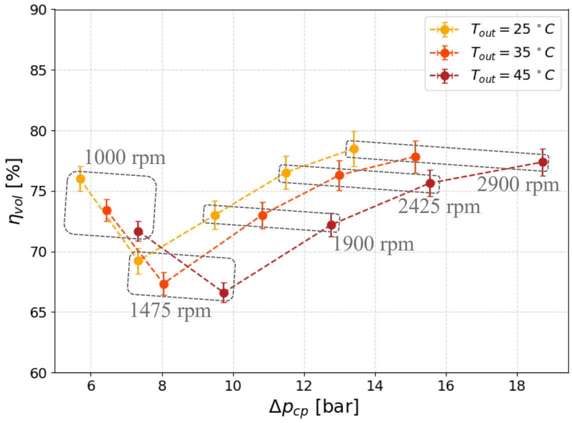

Figure 11. Volumetric efficiency vs. pressure difference for different outside temperatures (cooling mode)

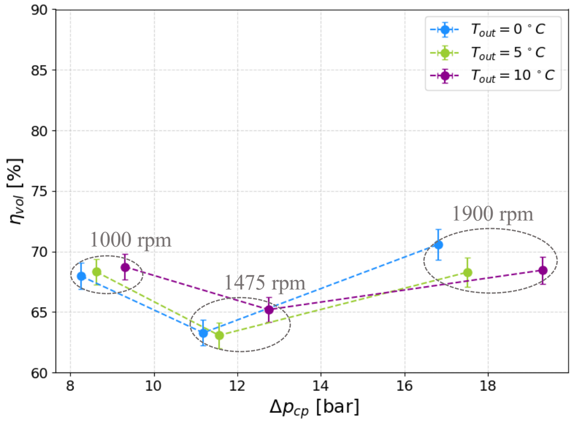

Figure 12. Volumetric efficiency vs. pressure difference for different outside temperatures (heating mode)

The uncertainty of the volumetric efficiency remains nearly constant across the investigated operating conditions, around 1%, as it mainly depends on the refrigerant mass flow rate measured by the Coriolis flow meter, whose uncertainty remains low over the operating range.

4. Conclusion and Future work

This paper presented a comprehensive experimental characterization of a reversible air-to-air heat pump system for a B-segment electric vehicle, conducted on a dedicated test bench designed as both a research and educational platform. Developed within a project-based learning framework, the bench enabled the experimental investigation of heating and cooling modes while providing students with hands-on experience in thermal system design, instrumentation, and data analysis.

The experimental campaigns highlighted the strong influence of operating conditions on system performance. In cooling mode, the coefficient of performance decreases from about 5 at a temperature lift of approximately 28 K to around 1.3 at 65 K. In heating mode, the COP decreases from about 3 at a temperature lift of 41 K to approximately 1.8 at 70 K.

Compressor performance was analyzed in terms of isentropic and volumetric efficiencies. The isentropic efficiency was shown to vary significantly with pressure ratio and compressor speed, with values typically ranging from approximately 40% to 60%. Volumetric efficiency is influenced by speed and pressure difference, decreasing at low speeds but increasing at higher speeds.

A detailed uncertainty analysis showed that the current measurement is the dominant source of uncertainty for COP and for the isentropic efficiency formulation based on electrical power, particularly at low compressor speeds, whereas temperature lift and volumetric efficiency uncertainties remain low.

The present work focuses on cabin thermal management. Battery cooling is not implemented in the current test bench configuration and is identified as a perspective for future work. Future developments will also include coupling the experimental results with numerical models to extend the analysis to a broader range of operating conditions and to support the optimization of electric vehicle thermal management systems, while further strengthening the educational value of the platform.

Nomenclature

Symbols

COP	Coefficient Of Performance	[-]	r_p	pressure ratio	[-]
h	specific enthalpy	[J/kg]	T	temperature	[K]
Δh	enthalpy difference	[J/kg]	$\dot{V}$	volume flow rate	$[m^3/s]$ or $[m^3/h]$
$\dot{m}$	mass flow rate	[kg/s]	V_s	swept volume	$[m^3]$
n	rotational speed	[tr/s]	$\dot{W}$	electrical power	[W]
p	pressure	[Pa]			
Δp	pressure difference	[bar]	ρ	density	[kg/m^3]
$\dot{Q}$	heat transfer rate	[W]	η	efficiency	[%]

Subscripts

cd	condenser	out	outlet
cp	compressor	ref	refrigerant
elec	electrical	sat	saturation
ev	evaporator	su	supply
id	ideal	vol	volumetric
is	isentropic		

Acronyms

AC	air conditioning
EV	electric vehicle
HP	heat pump
PWM	pulse width modulation

References

[1] ‘Greenhouse gas emissions from transport in Europe’. Accessed: Nov. 17, 2025. [Online]. Available: https://www.eea.europa.eu/en/analysis/indicators/greenhouse-gas-emissions-from-transport

[2] S. Kalweit, E. Zeyen, and M. Victoria, ‘Endogenous transformation of land transport in Europe for different climate targets’, *Energy Conversion and Management*, vol. 344, p. 120203, Nov. 2025, doi: 10.1016/j.enconman.2025.120203.

[3] M. Kılıç and M. Ö. Korukçu, ‘The Effect of Energy Management in Heating–Cooling Systems of Electric Vehicles on Charging and Range’, *Applied Sciences*, vol. 14, no. 15, p. 6406, Jan. 2024, doi: 10.3390/app14156406.

[4] A. König, S. Mayer, L. Nicoletti, S. Tumphart, and M. Lienkamp, ‘The Impact of HVAC on the Development of Autonomous and Electric Vehicle Concepts’, *Energies*, vol. 15, no. 2, p. 441, Jan. 2022, doi: 10.3390/en15020441.

[5] J. M. S. Jabardo, W. G. Mamani, and M. R. Ianella, ‘Modeling and experimental evaluation of an automotive air conditioning system with a variable capacity compressor’, *International Journal of Refrigeration*, vol. 25, no. 8, pp. 1157–1172, Dec. 2002, doi: 10.1016/S0140-7007(02)00002-6.

[6] M. Hosoz and M. Direk, ‘Performance evaluation of an integrated automotive air conditioning and heat pump system’, *Energy Conversion and Management*, vol. 47, no. 5, pp. 545–559, Mar. 2006, doi: 10.1016/j.enconman.2005.05.004.

[7] F. Qin, Q. Xue, G. M. Albarracin Velez, G. Zhang, H. Zou, and C. Tian, ‘Experimental investigation on heating performance of heat pump for electric vehicles at −20 °C ambient temperature’, *Energy Conversion and Management*, vol. 102, pp. 39–49, Sep. 2015, doi: 10.1016/j.enconman.2015.01.024.

[8] H. Zou, W. Wang, G. Zhang, F. Qin, C. Tian, and Y. Yan, ‘Experimental investigation on an integrated thermal management system with heat pipe heat exchanger for electric vehicle’, *Energy*

Conversion and Management, vol. 118, pp. 88–95, Jun. 2016, doi: 10.1016/j.enconman.2016.03.066.
[9] X. Tang, Q. Guo, M. Li, and M. Jiang, ‘Heating Performance Characteristics of an Electric Vehicle Heat Pump Air Conditioning System Based on Exergy Analysis’, *Energies*, vol. 13, no. 11, p. 2868, Jun. 2020, doi: 10.3390/en13112868.
[10] K. Li *et al.*, ‘Investigation on the performance and characteristics of a heat pump system for electric vehicles under extreme temperature conditions’, *Case Studies in Thermal Engineering*, vol. 27, p. 101308, Oct. 2021, doi: 10.1016/j.csite.2021.101308.
[11] J. Song *et al.*, ‘Experimental Study of an Air-Conditioning System in an Electric Vehicle with R1234yf’, *Energies*, vol. 16, no. 24, p. 8017, Dec. 2023, doi: 10.3390/en16248017.
[12] B. Guo, L. Zhao, J. Zhou, X. Sun, and Z. Yang, ‘Experimental investigation on the R1234yf air conditioning system with a battery cooling loop under realistic conditions of electric vehicles’, *Proceedings of the Institution of Mechanical Engineers, Part D: Journal of Automobile Engineering*, vol. 238, p. 095440702311569, Mar. 2023, doi: 10.1177/09544070231156953.
[13] J. Noguez and L. Neri, ‘Research-based learning: a case study for engineering students’, *Int J Interact Des Manuf*, vol. 13, no. 4, pp. 1283–1295, Dec. 2019, doi: 10.1007/s12008-019-00570-x.
[14] I. Wessels, J. Rueß, C. Gess, W. Deicke, and M. Ziegler, ‘Is research-based learning effective? Evidence from a pre–post analysis in the social sciences’, *Studies in Higher Education*, vol. 46, no. 12, pp. 2595–2609, Dec. 2021, doi: 10.1080/03075079.2020.1739014.
[15] M. Prince, ‘Does Active Learning Work? A Review of the Research’, *Journal of Engineering Education*, vol. 93, no. 3, pp. 223–231, 2004, doi: 10.1002/j.2168-9830.2004.tb00809.x.
[16] T. Gillet, ‘Étude expérimentale et modélisation numérique d’un système de climatisation multi-évaporateurs pour véhicule électrifié’.
[17] A. Possolo, ‘Simple Guide for Evaluating and Expressing the Uncertainty of NIST Measurement Results’, National Institute of Standards and Technology, NIST TN 1900, Oct. 2015. doi: 10.6028/NIST.TN.1900.
[18] F. Kaufmann, J. Von Zabienski, L. Von Ribbeck, M. Ehmann, H. Spliethoff, and C. Schifflechner, ‘Experimental Analysis of a Reversible High-Temperature Heat Pump/Orc Test Rig for Geothermal Chp Applications’, 2024, *SSRN*. doi: 10.2139/ssrn.5013851.